Appendix

Table A The associated Reynolds number under various turbulence intensities

Turbulence intensity, *u'* [m/s]	*Re* [-]
0.32 m/s	4704.446
0.65 m/s	9408.893
0.97 m/s	14113.34
1.29 m/s	18817.79
1.61 m/s	23522.23
1.94 m/s	28226.68
2.26 m/s	32931.12
2.58 m/s	37635.57
2.90 m/s	42340.02
3.22 m/s	47044.46
3.55 m/s	51748.91

Table B Calculated overall equivalence ratio

$\phi_{Ammonia}$	PMMA particles needed in the co-combustion field to maintain the total heat input identical to 0.3 kg/m^3 of the PMMA particle concentration [g]	Overall equivalence ratio by considering all PMMA particles being devolatilized [-]
0	1.8570	1.007
0.1	1.7594	1.057
0.2	1.6670	1.107
0.3	1.5794	1.157
0.4	1.4961	1.207
0.5	1.4170	1.258
0.6	1.3417	1.308
0.7	1.2699	1.358
0.8	1.2013	1.408
0.9	1.1359	1.458
1.0	1.0733	1.508
1.1	1.0134	1.558
1.2	0.9560	1.608

Table C The ratio of silica heat capacity to heat input in each $\phi_{Ammonia}$

$\phi_{Ammonia}$	Silica particle mass used for mixing combustion [kg]	Adiabatic flame temperature of ammonia–air flames[K]	Heat input by pure ammonia combustion [MJ]	Silica heat capacity under adiabatic flame temperature [MJ]	The ratio of silica heat capacity to heat input in each $\phi_{Ammonia}$ [-]
0.6	0.001342	1586.80	0.02122129	0.001582	0.074558
0.7	0.00127	1729.96	0.023796689	0.001632	0.068598
0.8	0.001201	1859.64	0.026179535	0.001659	0.063387
0.9	0.001136	1976.99	0.028390644	0.001669	0.058776
1.0	0.001073	2071.39	0.030447937	0.001651	0.054237
1.1	0.001013	2022.12	0.032366925	0.001522	0.047022
1.2	0.000956	1950.80	0.0341611	0.001386	0.040563

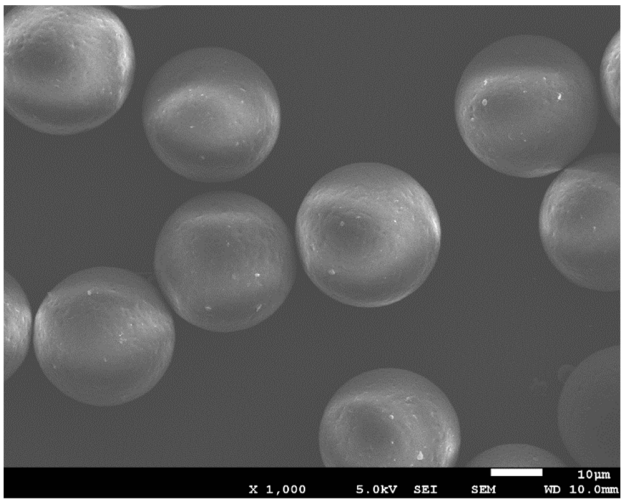

Fig. A Scanning electron microscopy (SEM) micrographs of the quasi-monodispersed PMMA particles

Table D The size distribution data for the 30 μm quasi-monodispersed PMMA particles

Size (μm)	Volume under (%)	Size (μm)	Volume under (%)	Size (μm)	Volume under (%)	Size (μm)	Volume under (%)	Size (μm)	Volume under (%)
0.01	0	0.182	0	2.98	0	60.256	100	1096.478	100
0.011	0	0.209	0	3.802	0	69.183	100	1258.925	100
0.013	0	0.24	0	4.365	0	79.433	100	1445.44	100
0.015	0	0.275	0	5.012	0	91.201	100	1659.587	100

0.017	0	0.316	0	5.754	0	104.713	100	1905.461	100
0.02	0	0.363	0	6.607	0	120.226	100	2187.762	100
0.023	0	0.417	0	7.586	0	138.038	100	2511.886	100
0.026	0	0.479	0	8.71	0	158.489	100	2884.032	100
0.03	0	0.55	0	10	0	181.97	100	3311.311	100
0.035	0	0.631	0	11.482	0	208.93	100	3801.894	100
0.04	0	0.724	0	13.183	0	239.883	100	4365.158	100
0.046	0	0.832	0	15.136	0	275.423	100	5011.872	100
0.052	0	0.955	0	17.378	0	316.228	100	5754.399	100
0.06	0	1.03	0	19.953	0	363.078	100	6606.934	100
0.069	0	1.259	0	22.909	5.33	416.869	100	7585.776	100
0.079	0	1.445	0	26.303	26.8	478.63	100	8709.636	100
0.091	0	1.66	0	30.2	66.77	549.541	100	10000	100
0.105	0	1.905	0	34.674	91.56	630.957	100		
0.12	0	2.188	0	39.811	99.96	724.436	100		
0.138	0	2.512	0	45.709	100	831.764	100		
0.158	0	2.884	0	52.481	100	954.993	100		

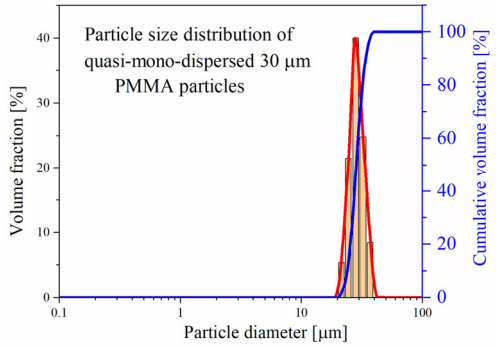

Fig. B Particle size distribution of the 30 µm quasi-monodispersed PMMA particles.

Table E Particle size characteristic parameters for the quasi-monodispersed PMMA particles which were manufactured by the Soken chemical Ltd

Particle size characteristic parameters	MX-3000 (Quasi-mono-dispersed 30 μm)
Volume weighted mean D [4,3] (μm)	28.813
Surface weight mean D [3,2] (μm)	28.297
Dv (10) (μm)	23.814
Dv (50) (μm)	28.521
Dv (90) (μm)	34.114
Specific surface area [m2/g]	0.212
COV (The coefficient of variation) [-]	0.117

Table F The size distribution data for the 46.1μm polydispersed silica particles

Size (μm)	Volume under (%)	Size (μm)	Volume under (%)	Size (μm)	Volume under (%)	Size (μm)	Volume under (%)	Size (μm)	Volume under (%)
2000	100	176	96.51	15.56	17.25	1.375	0	0.122	0
1826	100	161.4	96.1	14.27	15.66	1.261	0	0.111	0
1674	100	148	95.68	13.08	14.19	1.156	0	0.102	0
1535	100	135.7	95.25	12	12.82	1.06	0	0.094	0
1408	100	124.5	94.79	11	11.55	0.972	0	0.086	0
1291	100	114.1	94.28	10.09	10.38	0.892	0	0.079	0
1184	100	104.7	93.69	9.25	9.31	0.818	0	0.072	0
1086	100	95.96	92.98	8.482	8.35	0.75	0	0.066	0
995.6	100	88	92.1	7.778	7.49	0.688	0	0.061	0
913	100	80.7	90.98	7.133	6.73	0.63	0	0.056	0
837.2	100	74	89.52	6.541	6.06	0.578	0	0.051	0
767.7	100	67.86	87.59	5.998	5.46	0.53	0	0.047	0
704	100	62.23	85.05	5.5	4.93	0.486	0	0.043	0
645.6	100	57.06	81.73	5.044	4.45	0.446	0	0.039	0
592	100	52.33	77.56	4.625	4.01	0.409	0	0.036	0
542.9	100	47.98	72.47	4.241	3.6	0.375	0	0.033	0
497.8	100	44	66.63	3.889	3.22	0.344	0	0.03	0
456.5	99.95	40.35	60.25	3.566	2.86	0.315	0	0.028	0
418.6	99.84	37	53.71	3.27	2.52	0.289	0	0.026	0
383.9	99.66	33.93	47.4	2.999	2.2	0.265	0	0.023	0
352	99.42	31.11	41.59	2.75	1.89	0.243	0	0.021	0
322.8	99.15	28.53	36.53	2.522	1.59	0.223	0		
296	98.85	26.16	32.21	2.312	1.31	0.204	0		
271.4	98.51	23.99	28.61	2.121	1.04	0.187	0		
248.9	98.14	22	25.61	1.945	0.79	0.172	0		
228.2	97.74	20.17	23.08	1.783	0.56	0.158	0		
209.3	97.33	18.5	20.9	1.635	0.35	0.145	0		
191.9	96.92	16.96	18.98	1.499	0.14	0.133	0		

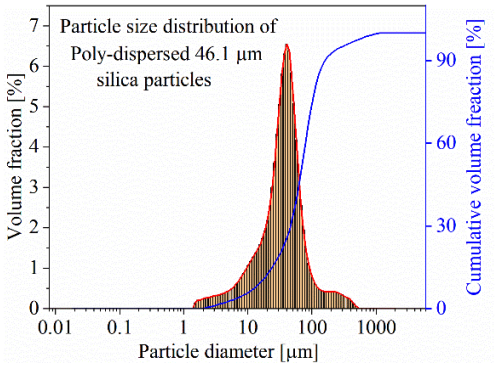

Fig. C Particle size distribution of the 46.1 µm polydispersed silica particles.

Table G The size distribution data for the polydispersed silica particles

Silica particles	Poly-dispersed silica particles
Mean volume diameter (µm)	46.08
Mean number diameter (µm)	2.6426
Mean area diameter (µm)	19.146
Specific surface area	0.31338
Standard deviation (µm)	22.961

The calculation of Stokes number

To understand the particle transport behaviors caused by the turbulence eddies in homogeneous isotropic turbulence flow, the authors calculated the Stokes number.

The Stokes number (*St*) [23], which is a very important dimensionless parameter in fluid–particle flow and can be calculated by the ratio of the particle response time to the characteristic timescale of the turbulent flow, was examined Stokes numbers for our experiments. The Stokes number related to the particle velocity is defined as Eq. (A) [23],

$$St = \frac{t_v}{t_f}. \tag{A}$$

where t_f is characteristic time of the flow field. If the $St << 1$, the response time of the particles is much less than the characteristic time associated with the flow field. Thus, the particles will have ample time to respond to changes in flow velocity. Consequently, the particle and fluid velocities will be nearly equal (velocity equilibrium). On the other hand, if the $St >> 1$, then the particle will have essentially no time to respond to the fluid velocity changes and the particle velocity will be little affected [23].

The response time of a particle or droplet to changes in flow velocity is important in establishing non-dimensional parameters to characterize the flow. The momentum response time relates to the time required for a particle or droplet to respond to a change in velocity. The momentum (velocity) response time, t_v, is estimated by Eq. (B) [23],

$$t_v = \frac{\rho_p d_p^2}{18\mu_g}. \tag{B}$$

where ρ_p is the particle density, d_p is the particle diameter and μ_g is the gas dynamic viscosity. In the present study, taking the ambient gas was air. The gas dynamic viscosity was calculated using the website of the Dandy research Group at Colorado State University [A]. By taking the ρ_p as 1200 kg/m³ and μ_g as 1.849×10^{-5} kg/(m·s), the PMMA particle relaxation time is estimated as 3.24 ms for 30 μm PMMA particles. For silica particles, the particle density is around 2000 kg/m³. Therefore, the relaxation time is estimated as 12.72 ms for 46.08 μm silica particle.

The characteristic time for the flow can be the longest time scale $t_{f\text{-}I} = L_f/u'$, the Taylor time scale $t_{f\text{-}T} = \lambda_f/u'$, and smallest time scale $t_{f\text{-}K} = \eta_k/u'$. L_f, λ_f, and η_k are turbulence longitudinal integral length scale, longitudinal Taylor length scale, and Kolmogorov length scale, respectively. The turbulence length scales were obtained from our previous research [13,21].

First, the characteristic time for the flow through a chamber can be the longest time scale $t_{f\text{-}I} = L_f/u'$, where L_f is the longitudinal integral length scale and u' is the turbulence intensity. It should be noted that the L_f is the largest length scale of the turbulent eddies in present experimental setup. The Stokes number then becomes,

$$St_I = \frac{t_v}{t_{f\text{-}I}} = \frac{t_v u'}{L_f}. \quad \text{(C)}$$

After some calculations, we obtained the values of Stokes number under different turbulence intensities by using integral time scale as the turbulence eddies time scale. As shown in Table H, all values of Stokes number are lower than or close to 1.

Table H The Stokes number based on the longitudinal integral time scale for particles under various turbulence intensities

Turbulence intensity, u' [m/s]	St_I for PMMA particle	St_I for silica particle

0.32 m/s	0.050072	0.196295
0.65 m/s	0.100145	0.392589
0.97 m/s	0.150217	0.588884
1.29 m/s	0.200289	0.785179
1.61 m/s	0.250362	0.981473
1.94 m/s	0.300434	1.177768
2.26 m/s	0.350507	1.374063
2.58 m/s	0.400579	1.570357
2.90 m/s	0.450651	1.766652
3.22 m/s	0.500724	1.962947
3.55 m/s	0.550796	2.159241

Besides, the characteristic time for the flow through a chamber can also be $t_{f\text{-}T} = \lambda_f/u'$, where λ_f is the longitudinal Taylor length scale and u' is the turbulence intensity. The Stokes number then becomes,

$$St_T = \frac{t_v}{t_{f\text{-}T}} = \frac{t_v u'}{\lambda_f}. \quad \text{(D)}$$

The λ_f was obtained based on Eq. (E) [13, 21].

$$\frac{\lambda_f^2}{L_f} = A_0 \cdot \frac{\mu}{u'}, \quad \text{(E)}$$

where A_0 is an empirical constant which was calculated by previous research [13], and A_0 was calculated as 18.5.

Table I The Stokes number based on the Taylor time scale under various turbulence intensities

Turbulence intensity, u' [m/s]	St_T for PMMA particle	St_T for silica particles

0.32 m/s	0.24183	0.948026
0.65 m/s	0.683998	2.681422
0.97 m/s	1.256584	4.926086
1.29 m/s	1.934638	7.584205
1.61 m/s	2.703739	10.59925
1.94 m/s	3.554157	13.93308
2.26 m/s	4.47875	17.55768
2.58 m/s	5.471983	21.45137
2.90 m/s	6.529404	25.59669
3.22 m/s	7.647329	29.9792
3.55 m/s	8.822645	34.5867

As shown in Table I, almost all values of the Stokes number, which calculated by using the Taylor scale as the turbulence eddies time scale, are larger than 1.

Besides, the characteristic time for the flow through a chamber can also be $t_{f\text{-}K} = \eta_k/u'$, where η_k is the Kolmogorov length scale and u' is the turbulence intensity. It should be noted that the η_k is the smallest length scale of the turbulent eddies. The Stokes number then becomes,

$$St_K = \frac{t_v u'}{\eta_K}. \tag{F}$$

The η_k was obtained from Eq. (G) [13,21],

$$\eta_k = \left(\frac{A_0}{15} \cdot \frac{\boldsymbol{\mu^3}}{u'^3} \cdot L_f\right)^{1/4}. \tag{G}$$

Table J The Stokes number based on the Kolmogorov time scale for quasi-monodispersed particle under various turbulence intensities

Turbulence intensity, *u' [m/s]*	St_K for PMMA particle	St_K for Silica particle
0.32 m/s	4.498568	17.63537
0.65 m/s	15.13132	59.31808
0.97 m/s	30.76355	120.5999
1.29 m/s	50.89548	199.5214
1.61 m/s	75.20934	294.8371
1.94 m/s	103.4758	405.6479
2.26 m/s	135.5176	531.2588
2.58 m/s	171.1913	671.1075
2.90 m/s	210.3772	824.7247
3.22 m/s	252.973	991.7098
3.55 m/s	298.89	1171.714

The procedure to obtain the turbulent flame propagation velocity

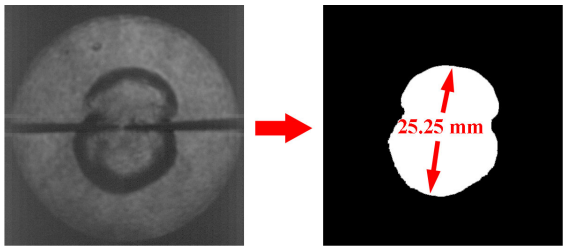

Fig. D schlieren image processing

As shown in Fig. D, to obtain the turbulent flame propagation velocity, the 16-bit schlieren images were processed by applying a threshold value to create gray levels ranging from 0 = black (flame) to 255 = white (background). Then, the images were converted to a binary image with a white flame and black background [1, 17–20]. The effects of changing threshold value on radius and velocity deviations were within ±2% [1]. Subsequently, the flame radii were determined by measuring the flame tips. As demonstrated by our previous research, while the turbulent flame radius calculated using the flame area method and directly measuring the flame tips are different, the radius calculation method has little effect on the exact value and basic tendency of the turbulent flame propagation velocity under different turbulence intensities [20]. Then, a polynomial relationship for the measured flame propagation radius as a function of time was applied to obtain the propagation velocity. Notably, the turbulent flame propagation velocity is just the flame front velocity relative to the ignition point. Further, Fig. E shows the turbulent flame radii and turbulent flame propagation velocity trajectories. The propagation velocities increased as the flame radius increased, which was consistent with prior findings in pure particle cloud combustion and solid particle cloud–ammonia co-combustion studies [17–20]. For comparison, the flame propagation velocities with a flame diameter of L_f were chosen. This methodology has been used in our previous solid and gas combustion studies [17–20, B–D]. This flame radius was chosen because it is equivalent to the flame diameter of 0.0209 m, which is the same length as the longitudinal length scale, L_f [17–21]. Turbulence longitudinal length scale is used to characterize the largest length scale of the turbulent flow

field. Therefore, in this flame diameter, the flame is considered to be affected by all eddies of the turbulent flow filed. Furthermore, as clarified by our previous research [20], the choice of the flame diameter has little effect on the conclusion.

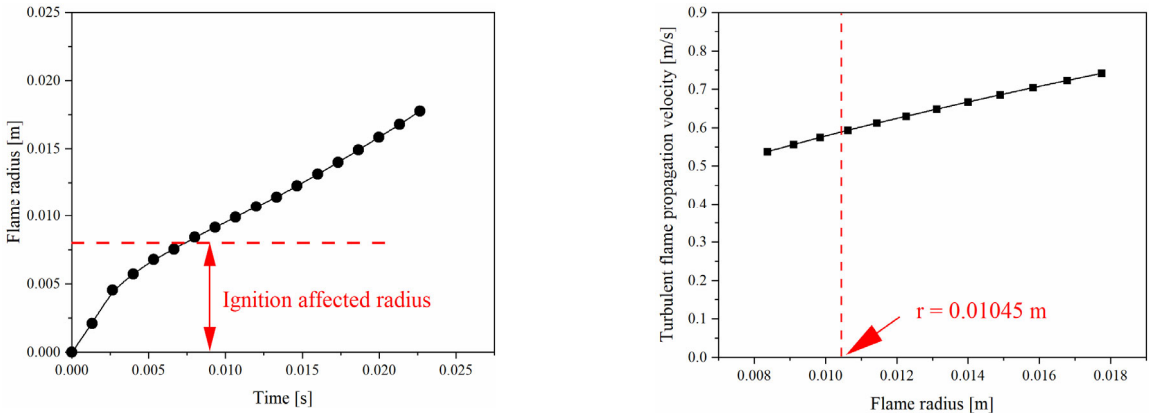

(a) Turbulent flame radii as a function of the time

(b) Turbulent flame propagation velocity as a function of the turbulent flame radius

Fig. E Turbulent flame trajectory in PMMA particle cloud–ammonia–air co-combustion under $\phi_{Ammonia}$ =0.1 and u' = 0.32 m/s

The calculation of particle devolatilization time scale of PMMA particle

To clearly clarify the particle devolatilization behavior in co-combustion, a simplified theoretical calculation of PMMA particle devolatilization time scale was conducted.

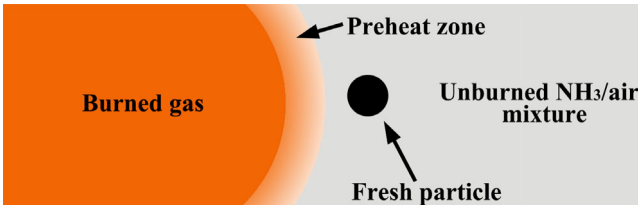

Fig. F The one-dimensional theoretical calculation model to obtain the PMMA particle devolatilization time scale

Figure F shows the theoretical model for the calculation of the particle devolatilization behavior. As shown in Fig. F, the flame propagates from left side to the right side. A particle is holding at the constant position. Then, the particle is preheated by the ammonia–air flame.

The particle temperature, $T_{p,}$ is calculated by considering the heat transfer due to convection, the heat loss due to the devolatilization reaction, using the following energy conservation equation [26, 27]:

$$m_p C_{p,\ p} \frac{dT_p}{dt} = -A_s h\left(T_p - T_g\right) - \Delta h_{dev} \frac{dV}{dt}. \quad \text{(H)}$$

where m_p is the particle mass, (kg). T_p is the temperature of the particle, (K). T_g is the surrounding gas temperature, (K). V is the mass of volatile matter that has been evolved from a PMMA particle, (kg). Δh_{dev} is the required heat for devolatilization, (J/kg). $C_{p,\ p}$ is the specific heat of particle, (J/kg/K). A_s is the surface area of the particle, (m^2). h is the convective heat transfer coefficient for the particles, ($W/m^2/K$)).

For the PMMA particle, there is no char reaction. The particle can be completely devolatilized. In the numerical simulation of the pulverized coal combustion field, the following formula that was proposed by Badzioch and Hawksley [27] is commonly employed for the modeling the devolatilization process:

$$\frac{dV}{dt} = K_v(mp), \tag{I}$$

$$K_v = A_v exp(-\frac{E_v}{RT_p}). \tag{J}$$

where A_v, E_v, R, and T_p are the pre-exponential factor for the volatile matter evolution rate equation (1/s), the activation energy for the volatile matter evolution rate (J/mol), gas constant (J/(mol K)) and the particle temperature (K).

Substituting Eq. (J) to Eq. (I), we obtained,

$$\frac{dV}{dt} = = A_v exp(-\frac{E_v}{RT_p})(mp) . \tag{K}$$

Finally, substituting Eq. (K) to Eq. (H), the energy balance equation goes into,

$$m_p C_{p,\,p} \frac{dT_p}{dt} = -A_s h\left(T_p - T_g\right) - \Delta h_{dev}(A_v exp(-\frac{E_v}{RT_p})\,(mp)) . \tag{L}$$

For the mass conservation equation, the decrease of the particle mass is equal to the increase of the amount of volatile matter. Then, the mass conservation equation can be written as Eq. (M),

$$\frac{dm}{dt} = -\frac{dV}{dt} = -A_v exp(-\frac{E_v}{RT_p})\,(m_p). \tag{M}$$

For the calculation of the T_g for Eq. (H), the simplified approach here follows that of Spalding [E, F].

Following assumptions were used for obtaining the T_g in the preheat zone.

(1) one dimensional, constant area, and steady flow.

(2) The kinetic and potential energies, viscous shear, thermal radiation were all neglected.

(3) The pressure is constant.

(4) The diffusion of heat and mass are governed by Fourier's and Fick's laws, respectively. Binary diffusion is assumed.

(5) the Lewis number is unity.

(6) the individual species specific heats are all equal and constant.

(7) fuel and oxidizer form products by a single step reaction.

For simplicity, we assume a simple linear temperature profile that goes from T_u to T_b over a distance of flame thickness, δ. Finally, we can obtain the following temperature distribution (Figure F).

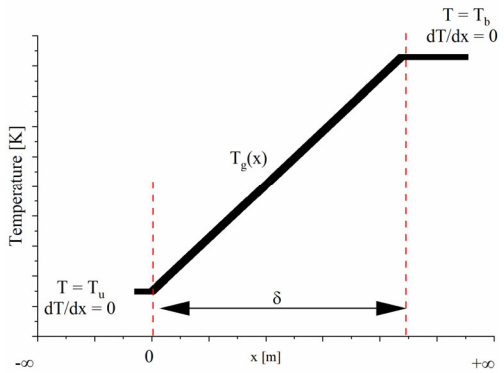

Fig. G Assumed temperature profile for laminar premixed flame analysis [E, F].

Based on Spalding and S.R. Turns, the $T_g(x)$ can be expressed as Eq. (N),

$$\frac{dT_x(x)}{dx} = \frac{T_b - T_u}{\delta}. \tag{N}$$

The flame thickness, δ, can be written as,

$$\delta = \frac{2k}{\rho_u c_p S_L}. \tag{O}$$

where k is the thermal conductivity, (W/m/K). ρ_u is unburned gas density, (kg/m^3). S_L is the laminar burning velocity of the premixed mixture, (m/s).

Therefore, substituting Eq. (O) to Eq. (N). $\frac{dT_x(x)}{dx}$ can be written as,

$$\frac{dT_x(x)}{dx} = \frac{(T_b - T_u)}{2k}(\rho_u c_p S_L). \quad \text{(P)}$$

Furthermore, considering the thermal expansion in the preheat zone due to the temperature increase, the ideal gas law was used,

$$PV = nRT \quad \text{(Q)}$$

The temperature increase can cause the volume increase in the preheat zone of flame front. Therefore, we can obtain,

$$V(x) = \frac{nRT(x)}{P}. \quad \text{(R)}$$

Finally, the mass in the preheat zone is constant. We can obtain,

$$\rho(x)V(x) = \rho(x=0)V(x=0). \quad \text{(S)}$$

Finally, we can obtain,

$$\rho(x) = \frac{\rho(x=0)V(x=0)}{V(x)}. \quad \text{(T)}$$

Substitute Eq. (R) to Eq. (T), we can obtain,

$$\rho(x) = \rho(x=0)\frac{T(x=0)}{T(x)}. \quad \text{(U)}$$

Finally, the density change in the x direction can be obtained.

Furthermore, based on above consideration, the relative velocity between particle and propagation wave of reaction front in the preheat zone can be considered as Eq. (V),

$$U(x) = \frac{\rho_b}{\rho(x)} S. \quad \text{(V)}$$

where S is the turbulent flame propagation velocity of flame at the flame radius of longitudinal integral scale, (m/s).

From above equation, we can obtain the $U(x)$ at each position of the x direction. Furthermore, the $U(x)$ can be treated as dx/dt. Using Euler method (dt = 0.000001 s), the $T_g(t)$ can be obtained. Then, the $T_g(t)$ was used for the calculation of the Eq. (H).

Furthermore, the Euler method (dt = 0.000001s) was used for the simultaneously solving Eq. (H) and Eq. (M). Finally, we obtained the particle mass (m_p) as function of the time under different ammonia equivalence ratios.

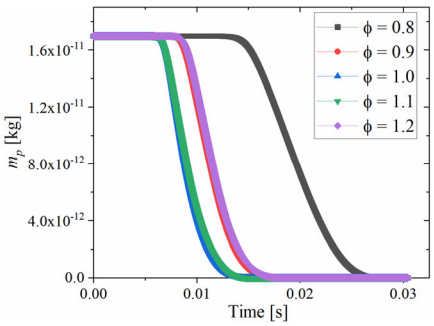

Fig. H Particle mass as a function of time.

The devolatilization time scale, t_{pyro}, is treated as the time needed for the complete devolatilization of the particle in the flame propagation process.

The calculation of the ammonia–air chemical reaction time scale

Further, the chemical time scale of pure ammonia combustion can be calculated by Eq. (W) [1],

$$t_a = \frac{\delta}{U_L}. \tag{W}$$

where δ is flame thickness and U_L is unstretched laminar burning velocity.

PMMA particle devolatilization time scale, ammonia–air chemical reaction time scale, and the ratio of two values

Finally, the PMMA particle devolatilization time scale, ammonia–air chemical reaction time scale, and the ratio of two values can be seen in table K.

Table K The PMMA particle devolatilization time scale, ammonia–air chemical reaction time scale, and the ratio of two values in PMMA particle cloud–ammonia–air co-combustion

$\phi_{Ammonia}$	t_a [s]	t_{pyro}[s]	t_{pyro}/t_a[-]
0.8	0.02679	0.02822	1.05323
0.9	0.01466	0.01784	2.43429
1.0	0.00933	0.01476	3.16389
1.1	0.00739	0.01520	4.11526
1.2	0.00947	0.01838	3.88125

The same method was used to obtain the t_{pyro}/t_a for the PMMA particle cloud–ammonia–oxygen–nitrogen co-combustion under an oxygen enriched condition (oxidizer: 40 % oxygen and 60% nitrogen). The associated values under an oxygen enriched condition can be seen in Table L.

Table L The PMMA particle devolatilization time scale, ammonia–oxygen–nitrogen chemical reaction time scale, and the ratio of two values in PMMA particle cloud–ammonia–oxygen–nitrogen co-combustion

$\phi_{Ammonia}$	t_a[s]	t_{pyro}[s]	t_{pyro}/t_a[-]
0.6	0.0017292	0.00974	5.632662503
0.8	0.0005656	0.008	14.14427157
1.0	0.000402	0.00737	18.33333333
1.2	0.000574	0.00781	13.60627178
1.4	0.0009906	0.00891	8.994548758

References

[1] Y. Xia, G. Hashimoto, K. Hadi, N. Hashimoto, A. Hayakawa, H. Kobayashi, O. Fujita, Turbulent burning velocity of ammonia/oxygen/nitrogen premixed flame in O2-enriched air condition, Fuel 268 (2020) 117383.

[13] R. Ichimura, K. Hadi, N. Hashimoto, A. Hayakawa, H. Kobayashi, O. Fujita, Extinction limits of an ammonia/air flame propagating in a turbulent field, Fuel 246 (2019) 178–186.

[17] Y. Xia, K. Hadi, G. Hashimoto, N. Hashimoto, O. Fujita, Effect of ammonia/oxygen/nitrogen equivalence ratio on spherical turbulent flame propagation of pulverized coal/ammonia co-combustion, Proc. Combust. Inst. 38 (2021) 4043–4052.

[18] Y. Xia, N. Hashimoto, O. Fujita, Turbulent flame propagation mechanism of polymethylmethacrylate particle cloud–ammonia co-combustion, Combust. Flame 241 (2022) 112077.

[19] K. Hadi, R. Ichimura, G. Hashimoto, Y. Xia, N. Hashimoto, O. Fujita, Effect of fuel ratio of coal on the turbulent flame speed of ammonia/coal particle cloud co-combustion at atmospheric pressure, Proc. Combust. Inst. 38 (2021) 4131–4139.

[20] Yu Xia, Nozomu Hashimoto, Turbulent flame propagation of polymethylmethacrylate particle clouds in an O_2/N_2 atmosphere, Combust. Flame 234 (2021) 111616.

[21] K. Hadi, R. Ichimura, N. Hashimoto, O. Fujita, Spherical turbulent flame propagation of pulverized coal particle clouds in an O_2/N_2 atmosphere, Proc. Combust. Inst. 37 (2019) 2935–2942.

[23] C.T. Crowe, J.D. Schwarzkopf, M. Sommerfeld, Multiphase Flow in Droplets and Particles, CRC press, Boca Raton, 2011.

[26] N. Hashimoto, R. Kurose, S.M. Hwang, H. Tsuji, H. Shirai, A numerical simulation of pulverized coal combustion employing a tabulated-devolatilization-process model (TDP model), Combust. Flame 159 (2012) 353–366.

[27] S. Badzioch, P.G.W. Hawksley, Kinetics of thermal decomposition of pulverized coal particles, Ind. Eng. Chem. Process Des. Dev. 9 (1970) 521– 530.

[A] D. Dandy, Bioanalytical Microfluidics Program, Color State Univ n.d., 2021 http://navier.engr.colostate.edu/code/code-2/index.html

[B] C. Mandilas, M.P. Ormsby, C.G.W. Sheppard, R. Woolley, Effects of hydrogen ad- dition on laminar and turbulent premixed methane and iso-octane–air flames, Proc. Combust. Inst. 31 (2007) 1443–1450.

[C] M. Lawes, M.P. Ormsby, C.G.W. Sheppard, R. Woolley, The turbulent burning velocity of iso-octane/air mixtures, Combust. Flame 159 (2012) 1949–1959.

[D] M. Fairweather, M.P. Ormsby, C.G.W. Sheppard, R. Woolley, Turbulent burning rates of methane and methane-hydrogen mixtures, Combust. Flame 156 (2009) 780–790.

[E] D. B. Spalding, Combustion and mass transfer, Pergamon, New York, 1979.

[F] S.R. Turns, An introduction to combustion: concepts and applications, The McGraw-HillCompanies, Inc., New York, 2012.